

## Magnetic properties of some rare earth magnesium compounds RMg<sub>2</sub>

Alois Loidl, K. Knorr, M. Müllner, K. H. J. Buschow

### Angaben zur Veröffentlichung / Publication details:

Loidl, Alois, K. Knorr, M. Müllner, and K. H. J. Buschow. 1981. "Magnetic properties of some rare earth magnesium compounds RMg<sub>2</sub>." *Journal of Applied Physics* 52 (3): 1433–38.  
<https://doi.org/10.1063/1.329776>.

### Nutzungsbedingungen / Terms of use:

licgercopyright

Dieses Dokument wird unter folgenden Bedingungen zur Verfügung gestellt: / This document is made available under these conditions:

#### Deutsches Urheberrecht

Weitere Informationen finden Sie unter: / For more information see:

<https://www.uni-augsburg.de/de/organisation/bibliothek/publizieren-zitieren-archivieren/publiz/>



RESEARCH ARTICLE | MARCH 01 1981

## Magnetic properties of some rare-earth magnesium compounds $\text{RMg}_2$


A. Loidl; K. Knorr; M. Müllner; K. H. J. Buschow




*J. Appl. Phys.* 52, 1433–1438 (1981)

<https://doi.org/10.1063/1.329776>






Lock-in Amplifier



Boxcar Averager



Zurich Instruments

Find out more

Boost Your Optics and Photonics Measurements

# Magnetic properties of some rare-earth magnesium compounds $\text{RMg}_2$

A. Loidl and K. Knorr

*Institut für Physik, Universität Mainz, Mainz, Federal Republic of Germany*

M. Müllner

*Institut für Kernphysik, Universität Frankfurt, Frankfurt, Federal Republic of Germany*

K. H. J. Buschow

*Philips Research Laboratories, 5600 MD Eindhoven, The Netherlands*

(Received 6 October 1980; accepted for publication 12 November 1980)

The magnetic properties of the compounds  $\text{PrMg}_2$ ,  $\text{NdMg}_2$ ,  $\text{DyMg}_2$ , and  $\text{ErMg}_2$  were studied by means of neutron diffraction at various temperatures. All these compounds give rise to ferromagnetic ordering. The absolute values of the magnetic moments in the magnetically ordered state are lower than the free-ion values. Inelastic neutron scattering at several temperatures was studied in  $\text{PrMg}_2$  and  $\text{NdMg}_2$ . Analysis of the scattering data in conjunction with the results of specific-heat and magnetization measurements shows that  $\text{PrMg}_2$  is an induced-moment system ( $\Gamma_3$  ground state), where quadrupolar effects carry a large weight in determining the magnetic properties. The values found for the crystal-field parameters in  $\text{PrMg}_2$  ( $x = 0.671$  and  $W = -0.345$ ) are consistent with the results obtained with  $\text{CeMg}_2$  and  $\text{NdMg}_2$  ( $A_4 > 0$ ,  $A_6 < 0$ ).

PACS numbers: 75.10 - b, 75.25. + z, 75.10.Dg, 65.40.Hq

## I. INTRODUCTION

In a previous investigation the magnetic properties of rare-earth magnesium compounds of the type  $\text{RMg}_2$  were studied by means of bulk magnetic measurements.<sup>1</sup> These compounds were classified as ferromagnetic, although indications were obtained from the peculiar temperature dependences of the magnetization that magnetic ordering might be more complex than ferromagnetic. In the present investigation we have studied the magnetic structure of the  $\text{RMg}_2$  compounds in more detail by means of neutron diffraction. Since the crystal structure of the  $\text{RMg}_2$  compounds changes from cubic ( $C15$ ) to hexagonal ( $C14$ ) in the middle of the series, we chose four representative examples ( $R = \text{Pr}$ ,  $\text{Nd}$ ,  $\text{Dy}$ , and  $\text{Er}$ ). Apart from neutron diffraction, the two cubic compounds  $\text{PrMg}_2$  and  $\text{NdMg}_2$  were also investigated by means of inelastic neutron scattering, in order to determine the energy-level scheme resulting from the splitting of the lowest  $J$  multiplet by the crystalline electrostatic field (CEF) of the surrounding ions.

## II. EXPERIMENTAL METHODS AND RESULTS

The samples of  $\text{PrMg}_2$ ,  $\text{NdMg}_2$ ,  $\text{DyMg}_2$ , and  $\text{ErMg}_2$  were prepared by sealing stoichiometric quantities of the elements into molybdenum containers and heating at  $1000^\circ\text{C}$  for several hours. Subsequently, they were annealed well above the peritectoid decomposition temperatures and finally quenched in water.

The neutron diffraction experiments were carried out on the multidetector diffractometer D1B at the Institut Laue-Langevin in Grenoble, France, with incident neutrons of a wavelength of  $2.516 \text{ \AA}$ . The samples of about 10 g each were enclosed in vanadium containers and fitted to a variable temperature cryostat. Powder patterns with scattering angles  $2\theta$  from 20 to  $100^\circ$  were taken well above and

below the Curie temperatures  $T_C$ . The intensity of some selected ferromagnetic Bragg reflections was followed through the magnetic phase transition. Figure 1 shows the diffracted neutron intensity of  $\text{ErMg}_2$  in the magnetically ordered phase ( $T = 3.7 \text{ K}$ ) and in the paramagnetic phase ( $T = 50 \text{ K}$ ), and the difference of the scattered intensities at the two temperatures [ $I(3.7 \text{ K}) - I(50 \text{ K})$ ]. Apart from three exceptions, all reflections above and below  $T_C$  can be indexed on the basis of the hexagonal unit cell of the  $C14$  Laves phases, indicating that the dimensions of the chemical and magnetic unit cell are the same. Three reflections (shaded areas in Fig. 1) could not be assigned to the  $C14$  phase. They are due to the parasitic phase  $\text{ErMg}$  (cubic,  $\text{CsCl}$  type), which is formed in the peritectic reaction or in the peritectoid decomposition of the compound. These extra reflections were left out of consideration in the following. The temperature dependence of the spontaneous magnetization shown in Fig. 2 was derived from the integrated intensities of the (100) and (101) reflections, which are of purely magnetic origin.

As a second example of the diffraction results we show in Fig. 3 the difference pattern  $I(2.4 \text{ K}) - I(130 \text{ K})$  of  $\text{DyMg}_2$ . Again the magnetic contributions are superimposed on the nuclear Bragg reflections. The appearance of a ferromagnetic (002) reflection indicates that, in contrast to  $\text{ErMg}_2$ , the direction of the magnetic moment does not coincide with the unique or  $c$  axis. In this case, too, traces of the parasitic  $\text{CsCl}$ -type phase were observed. The temperature dependence of the spontaneous magnetization was obtained from the (100), (002), and (101) powder lines. The results are presented in Fig. 4.

The diffraction experiments on the two cubic  $C15$  compounds  $\text{NdMg}_2$  and  $\text{PrMg}_2$  gave analogous results with exclusively ferromagnetic contributions to the difference powder patterns. In the diffraction pattern of the cubic compounds, parasitic lines (due to  $\text{CsCl}$ -type compounds) similar

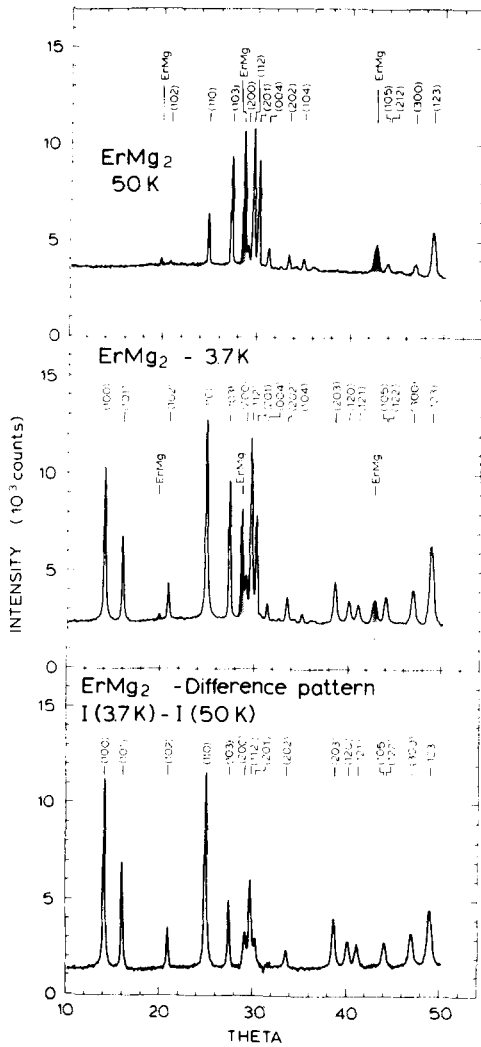


FIG. 1. Neutron diffraction patterns from  $\text{ErMg}_2$ .

to those in the hexagonal systems were present. The spontaneous magnetization curves shown in Figs. 5 and 6 were derived from the magnetic contributions to the (111) powder line, whose nuclear structure factor  $|F_{111}^{\text{nuc}}| \propto |b_{\text{RE}} - \sqrt{2}b_{\text{Mg}}|$  is small, because of the particular values of the scattering lengths  $b_{\text{RE}}$  and  $b_{\text{Mg}}$ .

In the quantitative analysis of the diffraction results the theoretical nuclear and magnetic structure factors were fitted to the integrated peak intensities of the experiment. In the Er and Dy compounds the latter quantities were corrected for a  $\theta$ -dependent absorption. Well-established theoretical values for the magnetic form factors were used. In addition,

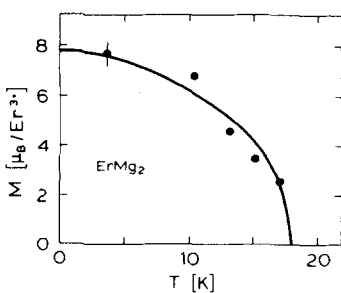


FIG. 2. Spontaneous magnetic moment of  $\text{ErMg}_2$ . The full line represents the Brillouin curve for  $J = 15/2$  with an effective Landé factor  $g^{\text{eff}} \approx 1.04$ .

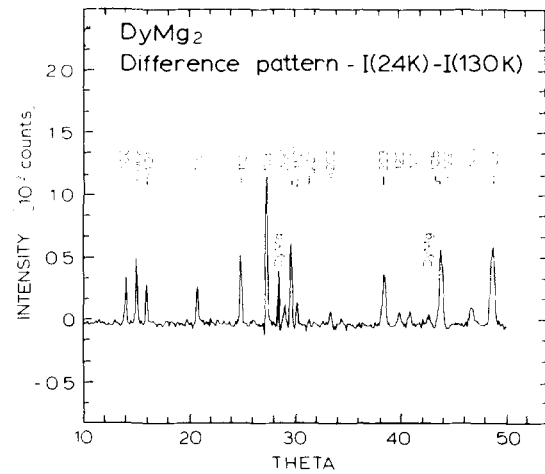


FIG. 3. Neutron diffraction pattern from  $\text{DyMg}_2$ .

tion, all the diffraction patterns of the cubic compounds and the nuclear powder lines of the hexagonal systems were analyzed utilizing the Rietveld method.<sup>2</sup> The fits yield the following relevant parameters (see also Table I): for C15 compounds, the lattice constants and the absolute values of the magnetic moments; for C14 compounds, the lattice constants, the absolute values of the magnetic moments, their angle with respect to the  $c$  axis, and the general coordinates  $x$  and  $z$  of the  $\text{Mg}(2)$  and RE atom positions, respectively. These coordinates were found to be  $x = 0.83$  and  $z = 0.062$ , which is in agreement with the tabulated values of the  $\text{MgZn}_2$  structure. The R factors of the fits of the integrated intensities fall into the range 5–10%.

The inelastic neutron scattering experiments on the two cubic compounds  $\text{NdMg}_2$  and  $\text{PrMg}_2$  were performed on the time-of-flight (TOF) spectrometer IN7 of the Institut Laue-Langevin. The incident neutron energies  $E_1$  and  $E_2$  were 14 and 56 meV, which, though simultaneously present, were well separated in the time of flight as first and second orders of the monochromator reflection. The neutron detectors covered scattering angles from 2.5 to 9 deg. The compound  $\text{NdMg}_2$  was studied at 30 K, which is just slightly above  $T_C$ . The part of the TOF spectrum next to the second-order elastic line is shown in Fig. 7. The spectrum is well described by a superposition of an elastic line of Gaussian shape and a quasielastic contribution of Lorentzian shape with a half-width  $\Gamma$  of 8 meV. Note the asymmetric profile of the quasielastic distribution which results from the thermal population fac-

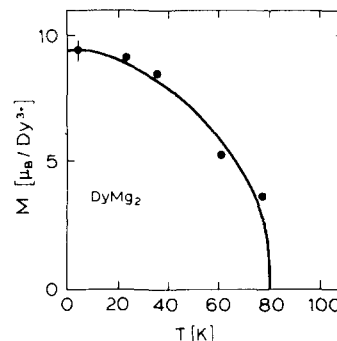


FIG. 4. Spontaneous magnetic moment of  $\text{DyMg}_2$ . The full line is the Brillouin curve for  $J = 15/2$  with an effective Landé factor  $g^{\text{eff}} = 1.24$ .

tor of the neutron scattering cross section. Individual peaks could not be resolved, not even with the lower first-order incident energy.

The measurements on  $\text{PrMg}_2$  were carried out at 14 and 100 K. Next to the second-order elastic line a transition with an energy transfer  $\Delta E = -16$  meV could be detected. At 100 K this transition is considerably reduced in intensity and a slight indication of the reverse transition appears at  $\Delta E = 16$  meV [Fig. 8(a)]. The range of the lower energy transfers is probed with improved resolution with the incident energy  $E_i = 14$  meV. Here the TOF spectrum at 14 K shown in Fig. 8b exhibits an intense quasielastic wing on the neutron energy loss side which extends to energy transfers up to about  $-3.5$  meV and which is followed by a peak at  $\Delta E = -4.5$  meV. At 100 K the TOF distribution has become more symmetrical and the structure at  $+4.5$  meV is almost washed out.

### III. DISCUSSION

In a previous investigation of the magnetic properties of  $\text{RMg}_2$  compounds the values of the magnetic moments measured at 4.2 K and 18 kOe were reported.<sup>1</sup> These values are considerably lower than those obtained by neutron diffraction in the present study (Table I). Two reasons for this difference can be given. In the first place the presence of a strong magnetocrystalline anisotropy leads to a preference in magnetization direction. It was mentioned previously that the moment alignment in our polycrystalline samples is still far from complete at 4.2 K and 18 kOe.<sup>1</sup> In the second place the magnetocrystalline anisotropy leads to a thermally activated magnetization process. Indications of this are found in the reported temperature dependences of the magnetization, where (for instance in  $\text{DyMg}_2$ ) a shallow maximum occurs below  $T_C$ .<sup>1</sup> At the lowest temperatures the magnetization values therefore correspond to values on a minor hysteresis loop; i.e., the magnetization reversal of the magnetic domains is still incomplete at 4.2 K and 18 kOe.<sup>3</sup> The present neutron diffraction results refute an explanation of these maxima in terms of a magnetic structure more complex than ferromagnetic.<sup>1</sup>

In all four compounds the ordered moments listed in Table I are still considerably lower than the free-ion values. We explain this moment reduction by a crystal-field splitting of the  $J$  ground multiplets. In the case of hexagonal symme-

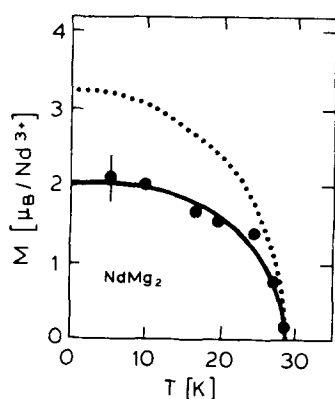


FIG. 5. Spontaneous magnetic moment of  $\text{NdMg}_2$ . The dotted line is the Brillouin curve for  $J = 9/2$ . The full line is the result of a mean-field calculation with the parameters  $x = 0.373$ ,  $W = 0.161$ , and  $\lambda = 141.3$  kG/ $\mu_B$ .

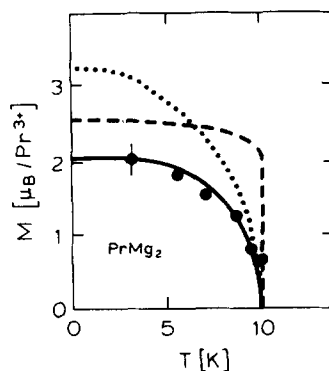


FIG. 6. Spontaneous magnetic moment of  $\text{PrMg}_2$ . The dotted line is the Brillouin curve for  $J = 4$ . The broken line gives the result of a mean-field calculation with  $x = 0.671$ ,  $W = -0.345$ , and  $\lambda = 117.5$  kG/ $\mu_B$ . The full line represents the theory including quadrupolar effects with  $\kappa = 13.3$  mK.

try the CEF is characterized by the multiple terms of second, fourth, and sixth order. Assuming that the second-order term  $A_2 \langle r^2 \rangle \alpha_2 \hat{O}_2^0$  is dominant, the directions of the magnetic moments observed in  $\text{DyMg}_2$  and  $\text{ErMg}_2$  are compatible with a negative coefficient  $A_2$  for both compounds. Then the change in sign of the Stevens factor  $\alpha_2$  from negative ( $\text{Dy}^{3+}$ ) to positive ( $\text{Er}^{3+}$ ) is responsible for the change of the easy axis from perpendicular to parallel with respect to the  $c$  axis.

In the case of cubic symmetry the CEF is described by the coefficients  $A_4$  and  $A_6$  of the fourth- and sixth-order terms or, alternatively, by  $x$  and  $W$ . (We have used the same notation as in Ref. 4.) In  $\text{PrMg}_2$  one might hope to obtain a precise knowledge of the CEF splitting since the neutron spectrum shows some structure and the measured temperature dependence of the specific heat<sup>1</sup> should add information for an analysis in terms of CEF effects. However, as we will show below, no consistent interpretation of all experimental data can be achieved as long as magnetic interactions in conjunction with mean-field theory are considered only. The selection of possible CEF schemes is guided by the TOF spectrum at 14 K. In principle, three details of the spectrum can be assigned to magnetic excitations: the quasielastic wing that peaks at 1.5 meV and the two transitions at 4.5 and 16 meV. However, the maximum number of magnetic dipole transitions out of the ground state of  $\text{Pr}^{3+}$  in a cubic CEF is only two, whatever the actual ground state is. Even if one assigns one of the structures of the TOF spectrum to a transition between excited CEF states, one cannot find any combination of the CEF parameters  $x$  and  $W$  which properly describes the observed excitation energies. We therefore ignore the low-energy peak at 1.5 meV for the moment and assume only two transitions out of the ground state with energy transfers of 4.5 and 16 meV. This assumption rules out a  $\Gamma_1$  ground state and leaves two solutions for the CEF parameters  $x$  and  $W$ : solution (A) with  $x = -0.805$  and  $W = -0.582$ , yielding a  $\Gamma_5$  ground state followed by  $\Gamma_3$  at 4.5 meV,  $\Gamma_4$  at 16 meV, and  $\Gamma_1$  at 32 meV; solution (B) with  $x = 0.671$  and  $W = -0.345$ , where the  $\Gamma_3$  ground state is followed by  $\Gamma_4$  at 4.5 meV,  $\Gamma_1$  at 10.8 meV, and  $\Gamma_5$  at 16 meV.

A mean-field calculation based on scheme (A) yields a second-order phase transition; the temperature dependence of the ordered moment follows a Brillouin-type law with a saturated moment of  $2.3 \mu_B$  (along  $[111]$ ), which is in fair agreement with the diffraction result. The calculated specific

TABLE I. Crystallographic and magnetic data of REMg<sub>2</sub> compounds. Lattice constants *a* and *c* at 4 K in Å; ordered magnetic moments in  $\mu_B$  per RE atom and ordering temperatures *T<sub>C</sub>* in K.

Structure			Ordered magnetic moment					
Compound	System	Type	<i>a</i>	<i>c</i>	<i>T<sub>C</sub></i>	Free ion	Observed	Magnetic axis
PrMg <sub>2</sub>	cubic	MgCu <sub>2</sub>	8.688(3)	...	10.0(0.5)	3.2	2.0(0.1)	
NdMg <sub>2</sub>	cubic	MgCu <sub>2</sub>	8.663(4)	...	28.5(1)	3.27	2.05(0.15)	
DyMg <sub>2</sub>	hex.	MgZn <sub>2</sub>	6.007(3)	9.745(4)	80.(7)	10.0	9.3(0.5)	⊥ to <i>c</i> axis
ErMg <sub>2</sub>	hex.	MgZn <sub>2</sub>	5.971(3)	9.680(4)	18.(1)	9.0	7.6(0.5)	<i>c</i> axis

heat is considerable larger than the measured one. This is best demonstrated by the values for the specific-heat jump at *T<sub>C</sub>*, which is calculated as about 2 R compared to the experimental value of 0.7 R. For scheme (A) the low-energy part of the neutron spectrum has to be interpreted as quasielastic scattering from transitions within the exchange-broadened  $\Gamma_3$  ground states, though the half-width of about 2 meV is unusually broad in relation to  $k_B T_C$ . In addition to the above discrepancies, the CEF parameter *A<sub>4</sub>* of solution (A) is opposite in sign with respect to CeMg<sub>2</sub> and to that in the isotypic series of REAl<sub>2</sub> compounds. On the other hand, the coefficient *A<sub>4</sub>* of scheme (B) agrees in sign with the closely related compounds; the parameters *x* and *W* are near to those of PrAl<sub>2</sub>.<sup>5</sup> They characterize PrMg<sub>2</sub> as a nonmagnetic ground-state system with an induced moment in the ferromagnetic phase. The polarization of the ground state occurs in such systems via the soft mode at the  $\Gamma$  point. An RPA calculation with an exchange coupling to the next nearest neighbors only (whose strength is determined by the value of *T<sub>C</sub>*) shows that the  $\Gamma_3$ – $\Gamma_4$  exciton is split into two branches and that the lower one, the acoustic branch, has softened at the zone center at 14 K to 1.0 meV, whereas at the zone boundary both

branches have energies close to the single-ion level separation of 4.5 meV. The low-energy part of the TOF spectrum can thus be explained qualitatively by the low-lying acoustic modes around the zone center whose weight is enhanced by the thermal population factor entering the neutron cross section. Molecular-field calculations for solution (B), where the bilinear magnetic interaction is characterized by the mean-field parameter  $\lambda = 117.5 \text{ kG}/\mu_B$ , predict a first-order phase transition at *T<sub>C</sub>* = 10 K and a saturated moment along [100] of 2.55  $\mu_B$  as shown by a broken line in Fig. 6. This obviously is in contradiction with the experiment. Related discrepancies exist for the magnetic contribution to the specific-heat capacity. With the same CEF parameters the magnetic heat capacity  $C/R = -T\delta^2\phi/\delta T^2$  was calculated via the Helmholtz free energy per rare-earth ion

$$\phi = \ln \sum_i \exp(-E_i/kT) + \lambda/2 \langle J_z \rangle,$$

using the same mean-field parameter as above i.e.,  $\lambda = 117.5 \text{ kG}/\mu_B$ . Although the calculated and measured entropy changes between 0 K and *T<sub>C</sub>* are in good agreement, the calculated specific heat concentrates too much in a  $\delta$ -like singularity at *T<sub>C</sub>*.

In the above considerations no account has been taken yet of the fact that the nonmagnetic ground-state  $\Gamma_3$  carries a substantial *E<sub>g</sub>* quadrupole moment. This means that the free energy has to be complemented by the term  $Q^2\kappa/2$ , where *Q* is the thermal average of the expectation value of  $3J_z^2 - J(J+1)$  and  $\kappa$  the corresponding mean-field parameter. By including this quadrupolar effect we were able to obtain simultaneously a good fit to the magnetization and specific-heat data. This is shown by means of the solid lines in Figs. 6 and 9. The value of the mean-field constant  $\kappa$  corresponding to these fits equals 13.3 mK. For  $\lambda$  we took the same value as above. It is interesting to note that with this combination of  $\kappa$  and  $\lambda$  values the magnetic and quadrupolar ordering temperatures coincide (at 10 K) and the magnetization is reduced with respect to the purely magnetic model. As can be seen from Fig. 6, this is the case in particular at the Curie temperature and just below it, where the jump in the magnetization has now largely disappeared. It follows from the above analysis that PrMg<sub>2</sub> is close to being tricritical. This feature is due to the interplay of the linear Stark splitting and the quadratic Zeeman splitting of the  $\Gamma_3$  state, which was discussed in detail by Ray and Sivadière.<sup>6</sup> Inspection of Fig. 9 shows that the Schottky or single-ion-type specific heat (solid line) gives a somewhat poor description of the experi-

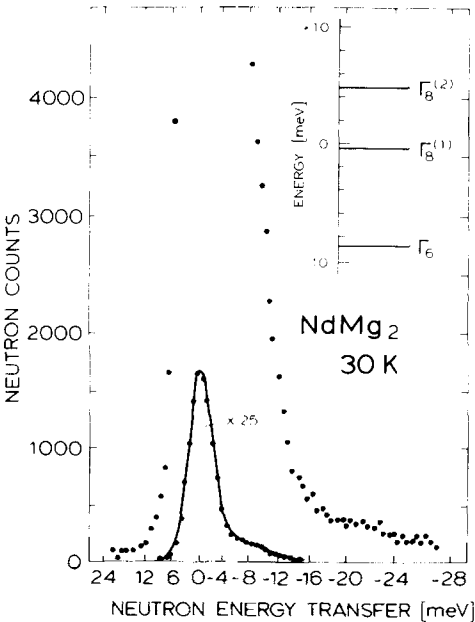


FIG. 7. TOF spectrum of NdMg<sub>2</sub> at 30 K (*E<sub>0</sub>* = 56.0 meV). The insert shows the crystal-field levels of NdMg<sub>2</sub>.

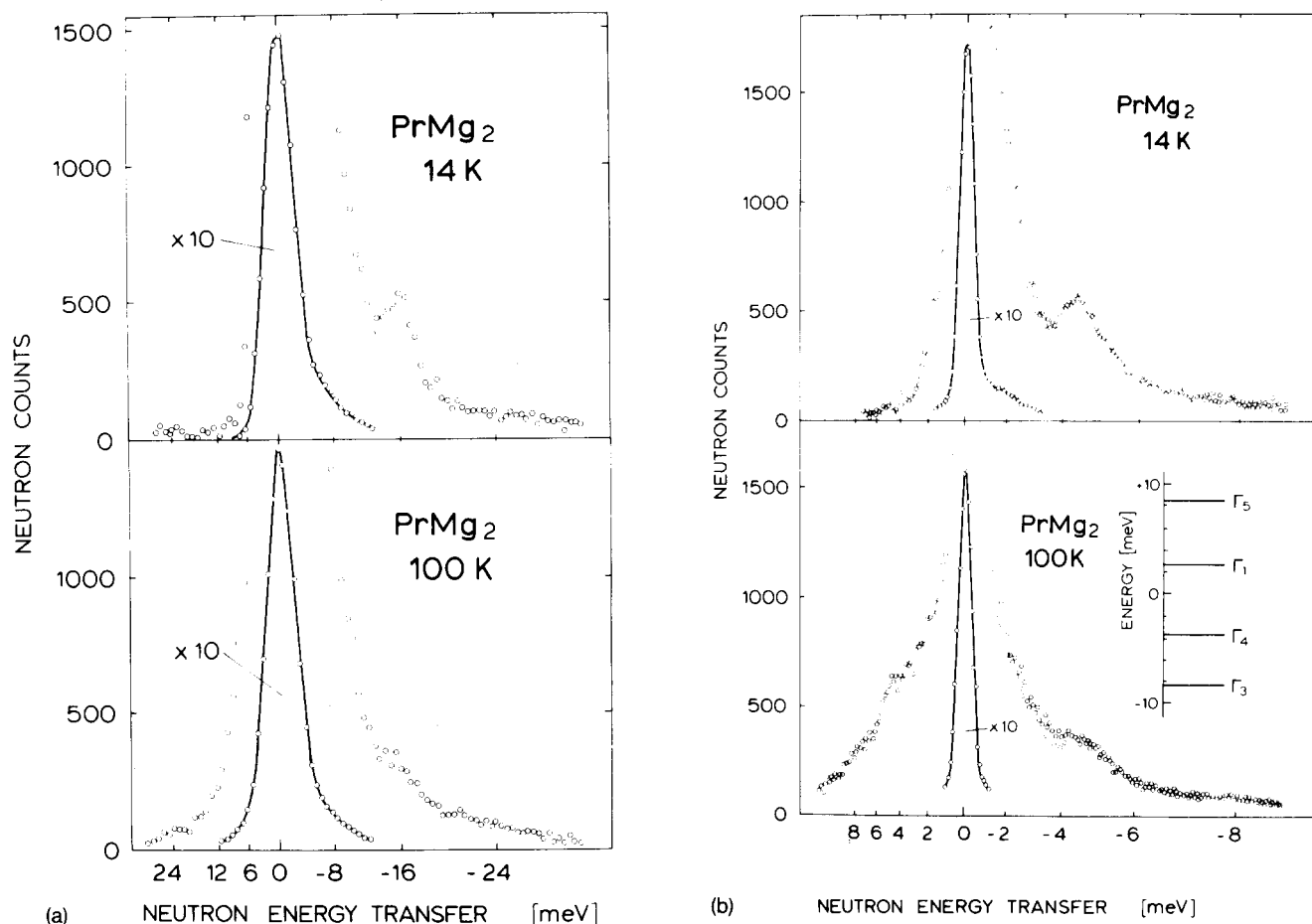


FIG. 8. TOF spectra of  $\text{PrMg}_2$  at 14 and 100 K, with (a)  $E_0 = 56$  meV and (b)  $E_0 = 14$  meV. The insert shows the crystal-field levels of  $\text{PrMg}_2$ .

mental results above  $T_C$ . Qualitatively this discrepancy can be explained by the presence of a soft  $\Gamma_3$ – $\Gamma_4$  exciton, as discussed above.

In  $\text{NdMg}_2$  the experimental information is considerably less than in  $\text{PrMg}_2$ . The absence of well-defined CEF transitions in the TOF spectra, in particular, hampers an analysis of the level scheme. All we can do is to check whether the data available can be explained by means of CEF parameters that are consistent with those found in  $\text{CeMg}_2$  and  $\text{PrMg}_2$ . For this reason we tried combinations with positive  $W$  and negative  $x$ , which is equivalent to positive  $A_4$  and negative  $A_6$  coefficients, since a positive  $A_4$  was derived<sup>1</sup> for  $\text{CeMg}_2$  and since a positive  $A_4$  was derived<sup>1</sup> for  $\text{CeMg}_2$  and since a positive  $A_4$  and negative  $A_6$  correspond to the combination  $x > 0$ ,  $W < 0$  derived above for  $\text{PrMg}_2$ . These conditions are furthermore also met in the CEF model of  $\text{NdAl}_2$ .<sup>4</sup> A mean-field calculation of the spontaneous magnetization of  $\text{NdMg}_2$  with this type of level scheme is shown as a solid line in Fig. 5. The dotted curve represents the Brillouin curve for  $J = 9/2$ . The CEF parameters  $x = -0.373$  and  $W = 0.161$  were used, the two excited  $\Gamma_8$  quartets then being at energies of 8 and 17 meV. This crystal-field level scheme is presented as an insert in Fig. 7. The ordered moment of  $2.05 \mu_B$  (along [100]) is achieved in molecular fields of about 300 kG.

In the inelastic neutron scattering experiment on

$\text{NdMg}_2$  at 30 K one would expect a single CEF transition  $\Gamma_6$ – $\Gamma_8^{(1)}$  at an energy transfer of  $-8$  meV. A quasielastic distribution with a half-width of 8 meV was observed instead. It is difficult to explain this result by a dispersive  $\Gamma_6$ – $\Gamma_8^{(1)}$  excitation the propagates through the lattice via the exchange coupling  $J(Q)$ , since the instability of the paramagnetic phase is mainly due to an alignment of the  $\Gamma_6$  ground-state moments and not to a renormalization of the  $\Gamma_6$ – $\Gamma_8^{(1)}$  Van Vleck susceptibility.  $\text{NdMg}_2$  is another example of the growing list of compounds where the inelastic neutron spectra have to be interpreted as being due to a scattering from overdamped CEF transitions. Quite generally the half-widths of these quasielastic distributions seem to be of the order of  $k_B T_C$  or of the order of the CEF splittings expected from an extrapolation of the CEF parameters of related compounds. A possible mechanism responsible for the damping of the CEF transitions has been given by Becker *et al.*,<sup>7</sup> who assume a scattering of the  $f$  electrons with conduction electrons which can be formally described by a frequency-dependent effective coupling  $J_{\text{eff}}(\omega)$  between the  $f$  states. We take these considerations as a support in choosing a separation of about 8 meV.

#### IV. CONCLUSION

We have shown by means of neutron diffraction that a representative number of  $\text{RMg}_2$  compounds give rise to fer-

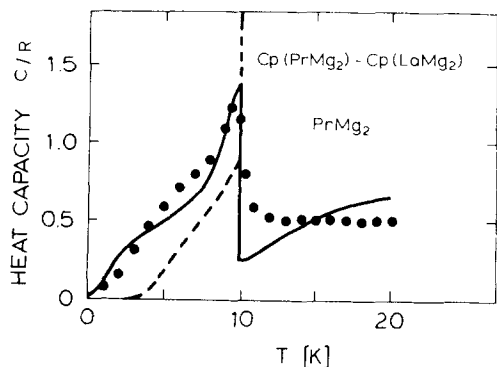


FIG. 9. Heat capacity of  $\text{PrMg}_2$ . Points: experimental data taken from Ref. 1; broken curve: theory with magnetic mean field only; full curve: theory including quadrupolar effects.

romagnetic ordering at low temperatures, so that the same will probably hold for the remaining compounds of this series, as already suggested by the results of magnetic measurements. The magnetic moments observed at low temperatures fall below the free-ion values as a result of the presence of crystalline electrostatic fields. In  $\text{PrMg}_2$  a satisfactory account of the temperature dependence of the spontaneous magnetization, the temperature dependence of the specific heat, and the results of inelastic neutron scattering could only be obtained by including in the analysis of these data a substantial interaction between the quadrupole moments associated with the crystal-field split ground state of the  $\text{Pr}^{3+}$  ions ( $\Gamma_3$ ). The sign of the crystalfield parameters shows a consistent behavior within the series  $\text{CeMg}_2$ ,  $\text{PrMg}_2$ , and  $\text{NdMg}_2$ . The same combination ( $A_4\langle r_4 \rangle > 0$  and  $A_6\langle r_6 \rangle > 0$ ) is also found in the isotopic series  $\text{RAl}_2$ . The parameters

obtained in this investigation for  $\text{PrMg}_2$  are even quantitatively quite close to those reported for  $\text{PrAl}_2$ . In view of the 8% difference in lattice constants and in view of the fact that the  $A_n\langle r_n \rangle$  values scale as  $a^n$ , this closeness is surprising. It probably means that the  $4f$  electrons feel the electrostatic field of the surrounding ions only indirectly and that the CEF interaction is mainly determined by the nature of the asymmetric charge distribution of the intra-atomic  $5d$  electron cloud.<sup>8</sup>

## ACKNOWLEDGMENTS

We thank A. P. Murani and G. Bomchil of the Institute Laue-Langevin, Grenoble, for their assistance during the neutron measurements. The first two authors gratefully acknowledge the support received of the BMFT of the Federal Republic of Germany.

<sup>1</sup>K. H. J. Buschow, R. C. Sherwood, F. S. L. Hsu, and K. Knorr, *J. Appl. Phys.* **49**, 1510 (1978).

<sup>2</sup>H. Rietveld, RCN Report 104, Reactor Centrum Nederland, Petten, The Netherlands (unpublished).

<sup>3</sup>B. Barbara, C. Bécle, R. Lemaire, and D. Paccard, *J. Phys. (Paris)* **32**, C1-229 (1971).

<sup>4</sup>K. R. Lea, M. J. Leask, and W. P. Wolf, *J. Phys. Chem. Solids* **23**, 1381 (1962).

<sup>5</sup>P. Bak, Risø Report 312, Risø, Denmark, 1974 (unpublished).

<sup>6</sup>D. K. Ray and J. Sivadière, *Phys. Rev. B* **18**, 1401 (1978).

<sup>7</sup>K. W. Becker, P. Fulde, and J. Keller, *Z. Phys. B* **28**, 9 (1978).

<sup>8</sup>G. Williams and L. Hirst, *Phys. Rev.* **185**, 407 (1969).